Influence of Welding Sequence on Welding Deformation of T-Joint

Yong Qin, Ziquan Jiao, Zhiqiang Feng, Nanhui Shi, Junfeng Han, and Xian Wei

Abstract Aiming at carbon dioxide gas shielded welding of T-groove of low carbon steel sheets in ship compartments, three practical welding processes were simulated by welding software Simufact Welding, and the effect of welding sequence on welding deformation was studied. The results show that the final deformation of cross-back-welding and simultaneous back-welding is smaller, while the process requirements of cross-back-welding are lower, which is most in line with the actual production requirements.

Keywords Simufact welding · CO_2 gas shielded welding · Cross-back-welding · Welding deformation

1 Introduction

Effective control of welding deformation is one of the key factors affecting the welding quality and production efficiency of components, and different welding methods, base metal properties, plate size, welding speed, welding sequence and thermal input have different effects on welding deformation.

This thesis mainly researches the cabin cubicle; its main function is to separate the space. Most of the plates are thick, and the joint form is T-joint without groove. At the same time, due to the large thickness of the base metal, the heat transfer is slow during welding, and the difference between the heat of the welded surface and the unwelded surface is large, which is easy to cause the angular deformation. Compared with the deformation correction of thin plate, the correction of thick plate is easier, but it will still increase the construction cost and prolong the construction period. Therefore, it is very important to choose a reasonable welding sequence [1].

Y. Qin
Guilin University of Electronic Technology, School of Mechanical and Electrical Engineering, 541004 Guilin, China

Y. Qin · Z. Jiao · Z. Feng (✉) · N. Shi · J. Han · X. Wei
Beibu Gulf University, College of Mechanical and Marine Engineering, 535011 QinZhou, China
e-mail: fzqsjtu@163.com

S. Chen et al. (eds.), *Transactions on Intelligent Welding Manufacturing*,
Transactions on Intelligent Welding Manufacturing,
https://doi.org/10.1007/978-981-15-6922-7_6

In this paper, the welding process is simulated by the professional welding software Simufact Welding 8.0, and the influence of welding sequence on the welding deformation of T-joint between cabin grids is studied. It provides relevant technical basis for accurate prediction of welding deformation of ship structure.

2 Establishment of Welding Model

2.1 Structural Model

In this study, the bottom bulkhead of the hull cabin is taken as the research object, and the SolidWorks software is used for modeling, which is composed of the bottom slab and eight bulkheads of the same size [2]. The actual size is shown in Fig. 1, the size of base plate is 6400 mm × 6000 mm × 20 mm, and the size of diaphragm is 400 mm × 6000 mm × 12 mm. Because the size of the original model is too large, in order to facilitate the mesh division and the subsequent simulation test, the model is simplified according to the symmetry, and only a combined model of diaphragm and base plate is studied. Because this paper is the fillet weld of T-joint without groove, the thickness of the welded plate is kept unchanged, the length and width of the plate are reduced proportionally, and the simplified model size is shown in Fig. 2. The base plate size is set as 300 mm × 800 mm × 20 mm, and the vertical plate is set as 60 mm × 800 mm × 12 mm.

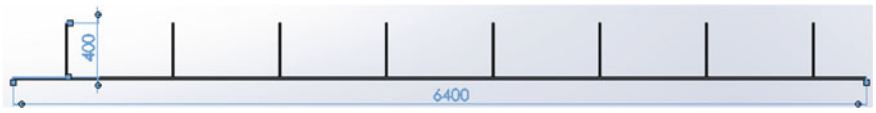

Fig. 1 Original geometric model

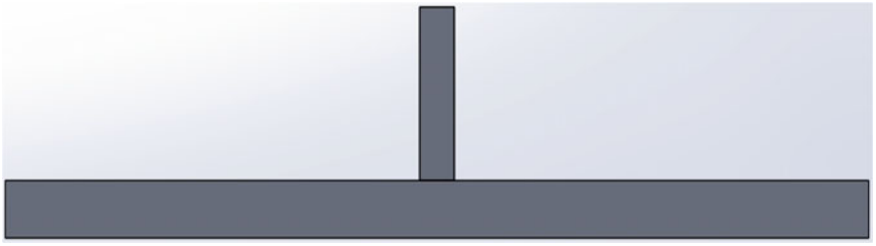

Fig. 2 Simplified geometric model of fillet welding

2.2 Technique Plan

The material used in the experiment is S355J2G3, which is a common low-alloy structural steel for ships. Its welding process can be regarded as a nonlinear transient heat transfer process with centralized input of heat source. During the welding process, the parameters such as heat transfer coefficient, thermal conductivity and specific heat capacity will change with the change of temperature and tend to be constant at a certain temperature, meeting the control equation of nonlinear transient heat transfer problem. It can be expressed as [3]:

$$\rho c \frac{\partial T}{\partial t} = \frac{\partial}{\partial x}\left(\lambda \frac{\partial T}{\partial x}\right) + \frac{\partial}{\partial y}\left(\lambda \frac{\partial T}{\partial y}\right) + \frac{\partial}{\partial z}\left(\lambda \frac{\partial T}{\partial z}\right) + Q_n \tag{1}$$

where ρ is the density of the material; c is the specific heat capacity of the material; λ is the thermal conductivity of the material; T is the instantaneous temperature of the material; Q_n is the heat generated inside the object.

The chemical composition and parameters of S355J2G3 low-carbon steel change with temperature as shown in Tables 1 and 2 [4, 5].

In the actual welding process, for the workpiece with a long weld, it is often used to control the welding deformation and other welding defects by means of sectional step back-welding, leap welding and other processes [6]. For example, the step back-welding process is to specify a large welding direction after a long workpiece is segmented, and the welding direction of each small section is opposite to the large direction. Step skip welding is the welding of each small segment along the general direction of welding, while welding is not carried out in accordance with the sequence, as shown in Fig. 3. These two technologies can effectively control the welding deformation and improve the welding efficiency.

Table 1 Chemical composition of low-carbon steel

Element	C	Si	Mn	P	S	Nb	V	Ti	Cr	Ni	Cu	N	Mo
Content max (%)	0.2	0.5	1.7	0.035	0.035	0.07	0.15	0.2	0.3	0.5	0.3	0.012	0.1

Table 2 Material property parameters of low-carbon steel changing with temperature

Temperature T (°C)	20	200	400	600	800	1000	1300	1842	2227
Density P (kg/m^3)	7820	7740	7710	7650	7620	7580	7500	7200	7200
Specific heat capacity c (J/kg · °C)	460.0	491.7	557.8	667.1	1108.0	626.4	637.9	645.5	645.5
Thermal conductivity λ (J/m · s · °C)	50.0	51.1	44.4	39.4	31.8	26.4	29.7	105	105
Heat transfer hc (J/m^2 · s · °C)	1.00	1.50	1.70	1.86	1.98	2.09	2.22	2.29	2.32

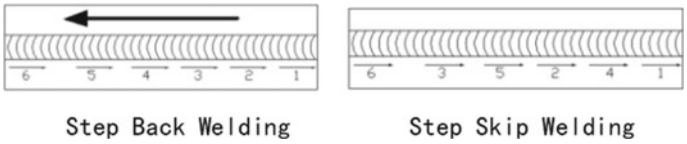

Fig. 3 Step back-welding and step skip welding

In fillet welding of structural parts with large thickness and no bearing force, the welding process without groove and without penetration is often adopted. Therefore, the welding joint of this paper is the fillet weld of T-joint without groove. Three schemes are adopted to study the welding deformation law.

As shown in Fig. 4, the following scheme is adopted to study the welding deformation law, and the numbers in the figure are the welding sequence.

In scheme 1, adopting step cross-back-welding, the welding direction of each section is opposite to the general welding direction, and the process of left and right cross-welding is adopted.

The second option is the process of no cross-sectional welding. The welding direction of each section is opposite to the general welding direction, but the welding is carried out from left to right.

In scheme 3, the welding shall be carried out in sections at the same time. There is no long cooling time between each welding process of the three schemes, and the same cooling is carried out after the final welding of all cooling.

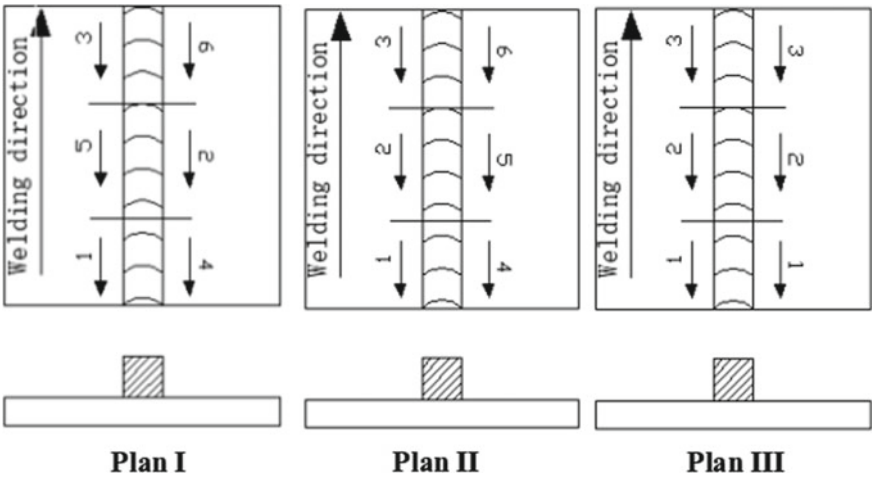

Fig. 4 Welding process plan

3 FEM Analysis Model

3.1 Heat Source Model

There are many kinds of welding heat source models. Different heat source models are selected according to different welding structures, material specifications, plate thickness and welding methods. At present, the best choice is ellipse heat source model, double-ellipse heat source model and Gauss heat source model. According to the symmetry of the welding seam, the key points can only be selected from half of the base metal. Using double-ellipse model to load heat source can better carry out numerical simulation, and the simulation results are closer to the measured results [7].

Goldark's double-ellipse heat source model overcomes the shortcomings of different heat source gradients in the front and rear hemispheres of the ellipse heat source model, that is, the temperature gradients in the first half of the ellipse heat source model are not as steep as the actual temperature gradients, and the temperature gradients in the second half are relatively slow [8]. The double-ellipse heat source model is shown in Fig. 5.

The first half of the double-ellipse heat source model is a one-fourth ellipsoid model, and the second half is another one-fourth ellipsoid model. Then, the heat source model distribution expression of the first half ellipsoid is:

$$q(r) = \frac{6\sqrt{3} f_1 Q}{\pi^{3/2} a_r bc} \exp\left\{-3\left[\left(\frac{x}{a_r}\right)^2 + \left(\frac{y}{b}\right)^2 + \left(\frac{z}{c}\right)^2\right]\right\} \tag{2}$$

The distribution expression of heat source model for the second half ellipsoid is:

$$q(r) = \frac{6\sqrt{3} f_2 Q}{\pi^{3/2} a_f bc} \exp\left\{-3\left[\left(\frac{x}{a_f}\right)^2 + \left(\frac{y}{b}\right)^2 + \left(\frac{z}{c}\right)^2\right]\right\} \tag{3}$$

where f_1 and f_2 are the distribution functions of heat flux density, respectively, and $f_1 + f_2 = 2$; Q is the input heat source power and $Q = \eta U I$; at the same time,

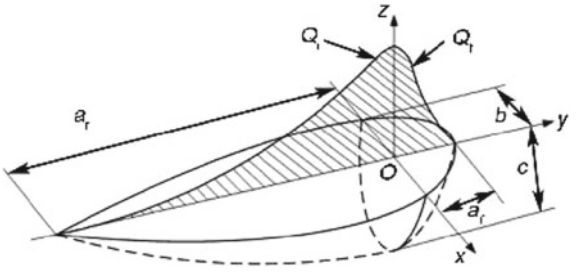

Fig. 5 Double-ellipse heat source model

a_r, a_f, b and c are the parameters of defining ellipse, which have no influence on each other and can take different values.

In this paper, the simulation is based on Simufact Welding 8.0 software, which only needs to be based on the size of the weld pool and the actual welding process. In addition, the simulated heat source model needs to wrap 3–5 grids in each direction of the weld area to simulate accurately. Therefore, the numerical selection of A, B and C can be made according to the size of the weld pool obtained in the ideal state by using the backward method.

3.2 Parameter Configuration and Analysis Calculation

As shown in Fig. 6, the weldment is divided into weld zone, near weld zone and base metal zone according to the effect of welding heat on base metal. In order to facilitate the calculation, the grid size of the weld area is set to 2 mm, and the near weld area and the base metal area are combined. The grid is divided by dense and sparse grid, so as to minimize the number of grid. The number of final volume grid cells is 168,000, and the number of nodes is 201,000.

This thesis mainly researches the actual welding process of CO_2 gas shielded welding at room temperature 20 °C is simulated. According to the welding process and the thickness and size of the plate, the welding current and voltage are set as 360 A and 35 V, the thermal efficiency is 0.8. The parameters of the Gaussian double-ellipse heat source model are set, the front section is 5 mm, the back end is 15 mm long, the width is 9 mm, the depth is 12 mm, and the parameters of the Gaussian heat source are 3. As shown in Fig. 7, the weld adopts triangle shape, which is automatically generated by the software. "a" refers to the depth of weld and the height of the triangle, "*b*" refers to the reinforcement and can be raised or concave, Z_1 and Z_2 refer to the weld fillet size, $Z_1 = Z_2$ is set as 5 mm, $b = 0$ mm, and "*a*" dimension is automatically generated as 3.53553 mm. Figure 8 shows the automatically generated weld shape.

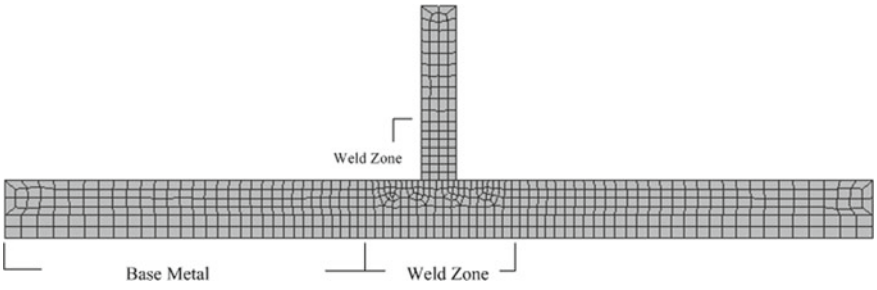

Fig. 6 Mesh generation plan

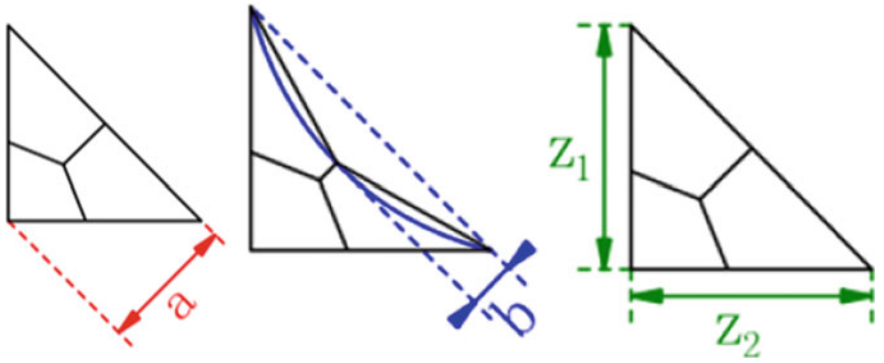

Fig. 7 Weld size definition

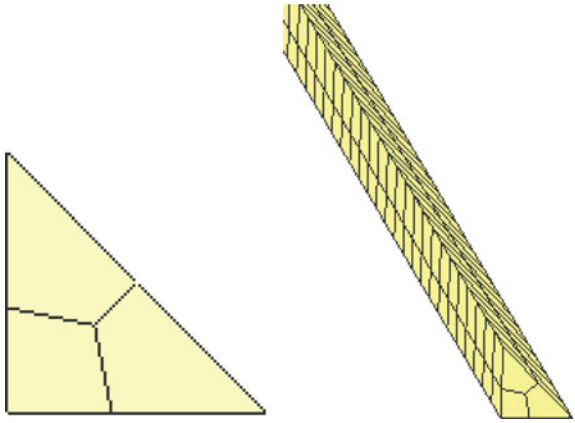

Fig. 8 Geometric model of weld

As shown in Fig. 9, boundary conditions are defined. One base plate located on four corners was four clamping devices; Q345 steel, S355J2G3, corresponding to the software, were selected as the base material, weld material and welding wire material. In particular, this simulation does not prevent rigid fixation at the four corners of the bottom plate, which is to study the state of the bottom plate warping after welding to a greater extent.

4 Analysis of Simulation Results

4.1 Result Analysis of Scheme 1

Observe the simulation results under the condition of three times magnification, as shown in Fig. 10 is the deformation of base metal after the first three sections of

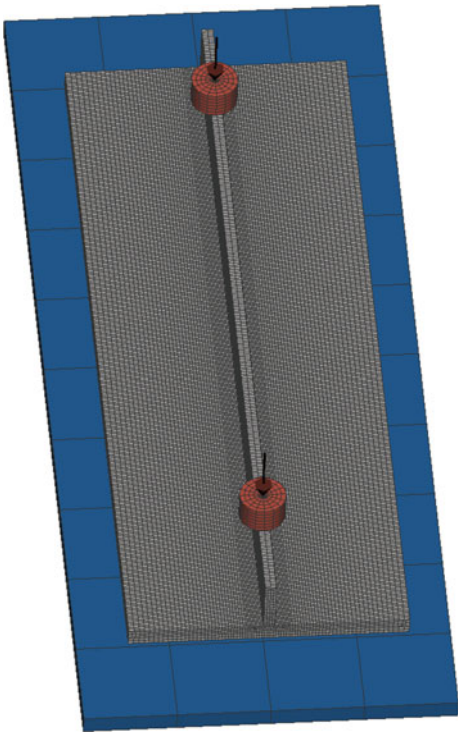

Fig. 9 Define boundary conditions

welding. The diaphragm is distorted. Because in the process of segmented back-welding, there is a large gap between the two sides of the baffle plate. As shown in Fig. 11, after the completion of the six-section welding, the distortion of the diaphragm basically recovers, and there is no obvious distortion under three times magnification. In scheme 1, before the welding is finished and the cooling and heat release step is started, the cross section along the z-axis is magnified by three times, and it can be seen that there are different degrees of deformation on the y-axis and x-axis. Among them, both ends of the bottom plate are obviously raised.

With the increase of cooling time, the deformation of the four corners of the bottom plate decreases as the base metal temperature approaches to room temperature. As shown in Figs. 12 and 13, they are the deformation of the bottom plate when cooling for 8 min and 15 min, respectively. The deformation trend gradually spreads to the two points (upper left corner) at the end of the weld, and the deformation at both ends of the first end of the weld gradually decreases. According to the actual welding process, the thicker the base metal, the longer the cooling time to room temperature. The maximum deformation position of the final base metal is at the end of the last welding section.

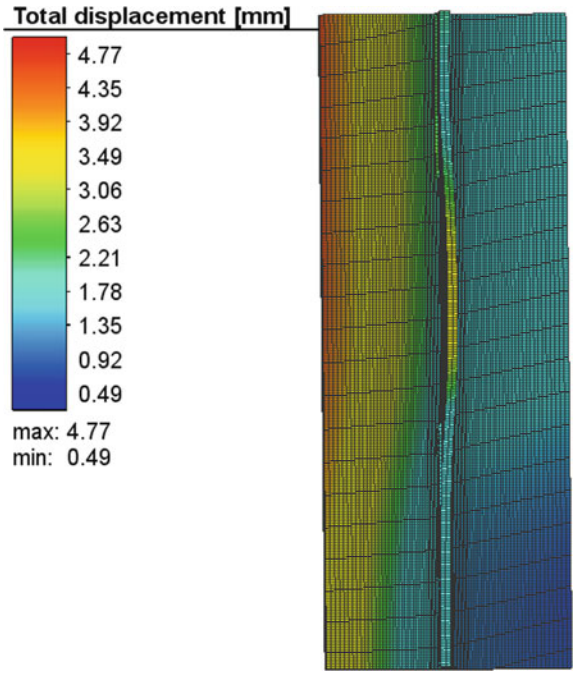

Fig. 10 Front three sections of diaphragm are twisted and deformed after welding

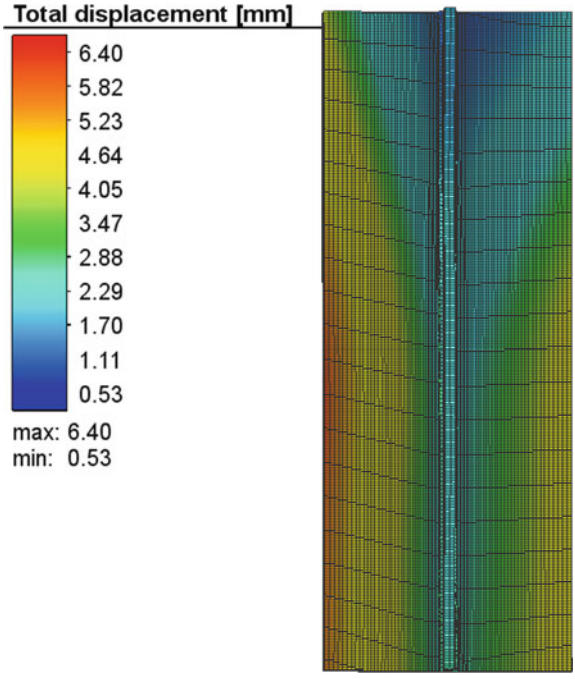

Fig. 11 Baffle plate is twisted and deformed after welding

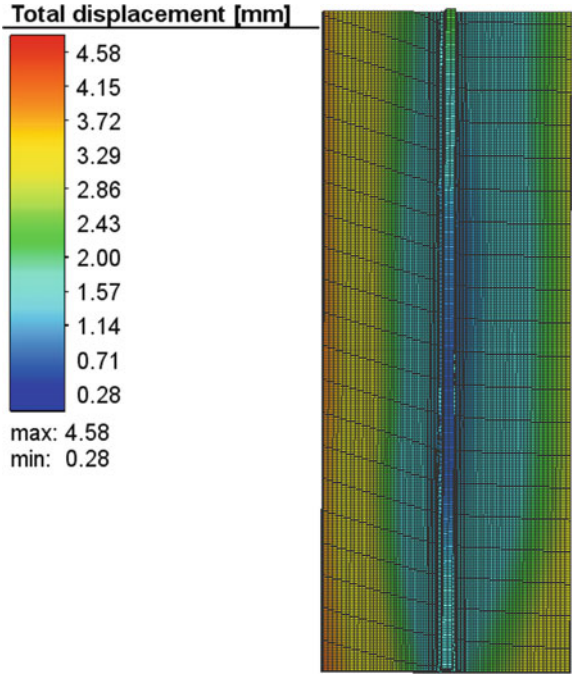

Fig. 12 Diagram of deformation after cooling for 8 min

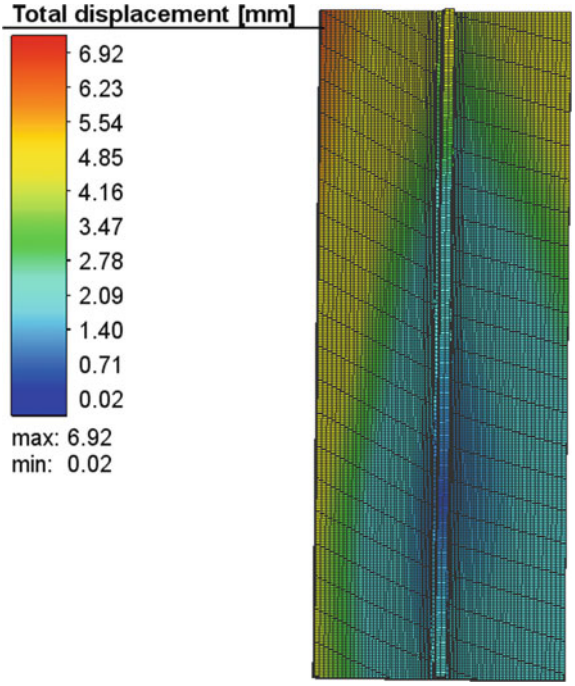

Fig. 13 Diagram of deformation after cooling for 15 min

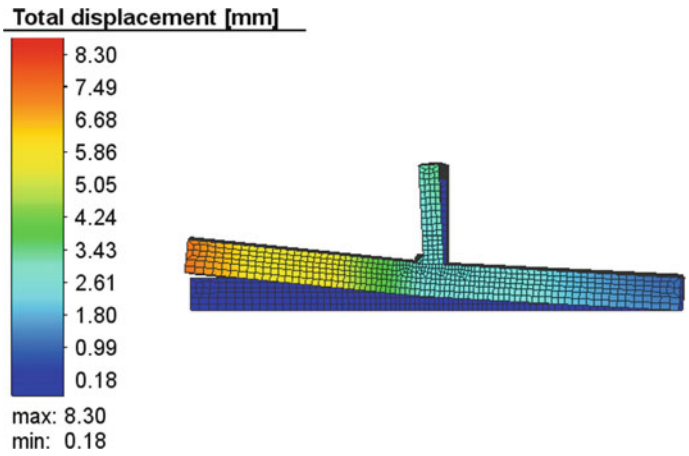

Fig. 14 Angular distortion of the first three sections after welding

4.2 Result Analysis of Scheme 2

Observe the simulation results under the condition of three times magnification, as shown in Fig. 14 is the deformation of base metal after the first three sections of welding are completed. The distortion of the diaphragm is small, but the angle between the base plate and the diaphragm is serious. Because the first three sections of welding only act on the same side, the temperature distribution in the thickness direction of the plate is uneven, the welding side has a large thermal expansion, and the expansion on the other side is small, which leads to the expansion of the welding side being hindered and serious transverse compression deformation. As shown in Fig. 15, the deformation state at the end of all welding is shown. The right bottom plate has a small up-warping, the partition plate returns to a vertical state, and the angular deformation is small. Because the welding temperature on the left side is too high, it is equivalent to preheating the welding on the right side, so that the temperature difference on the right side is low and the deformation is small.

With the increase of cooling time, when the temperature of base metal approaches to room temperature, the elastic deformation and plastic deformation in the base metal tend to be stable, and the overall deformation does not change much. As shown in Fig. 16, the deformation state after final cooling. Serious angular deformation occurs on the right side, large floor warping, no obvious left floor warping, small deformation.

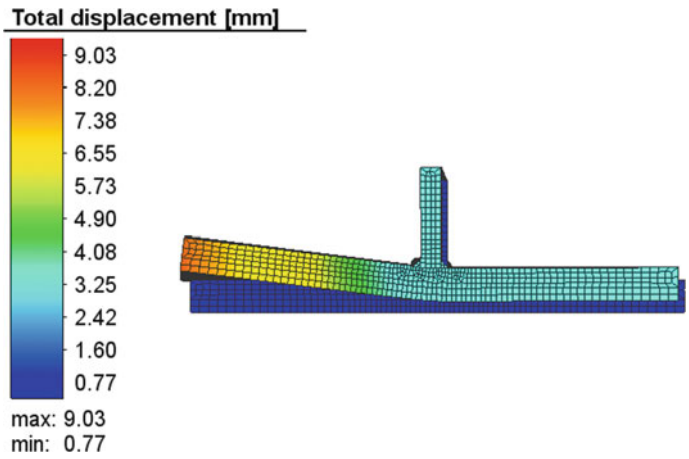

Fig. 15 Angular distortion after welding

Fig. 16 Schematic diagram after cooling

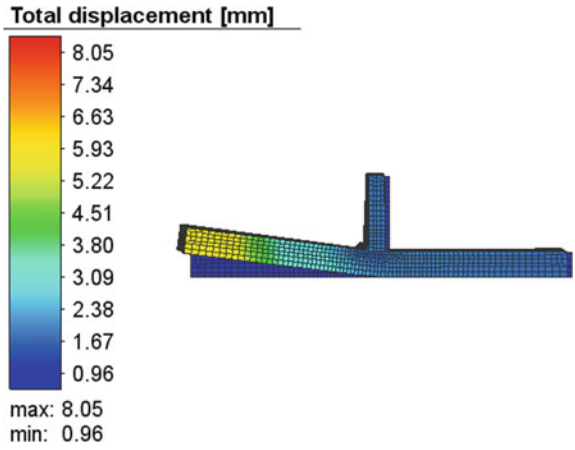

4.3 Result Analysis of Scheme 3

As shown in Fig. 17, the welding process flowchart of scheme 3, the change and migration rule of deformation can be seen. The deformation at both ends of the base plate is the largest, and the maximum deformation also changes with the moving direction of the welding. As shown in Figs. 18 and 19, the total deformation of cooling for 8 min and cooling for 15 min respectively. At this time, the temperature of the base metal is close to room temperature, and the elastic deformation in the base metal is gradually reduced, and the deformation is stable.

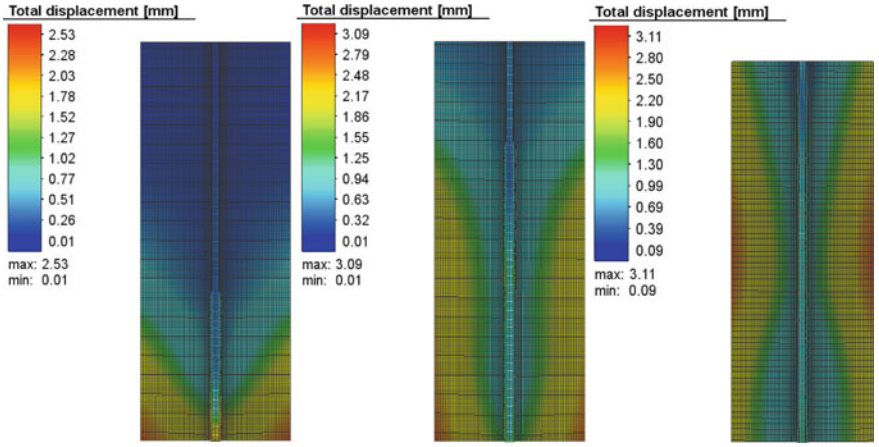

Fig. 17 Welding process deformation flowchart

Fig. 18 Diagram of deformation after cooling for 8 min

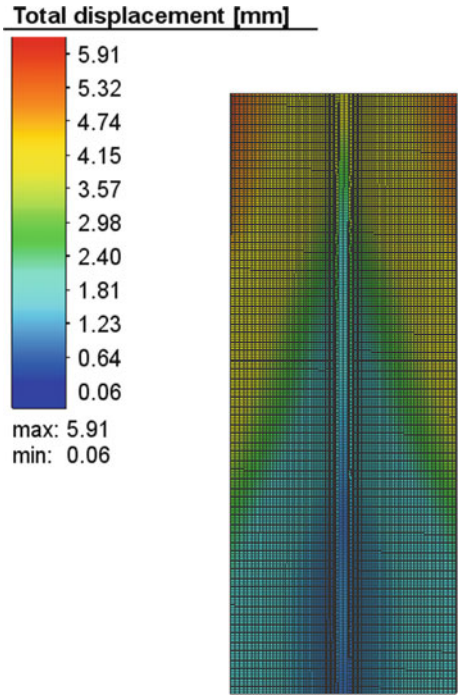

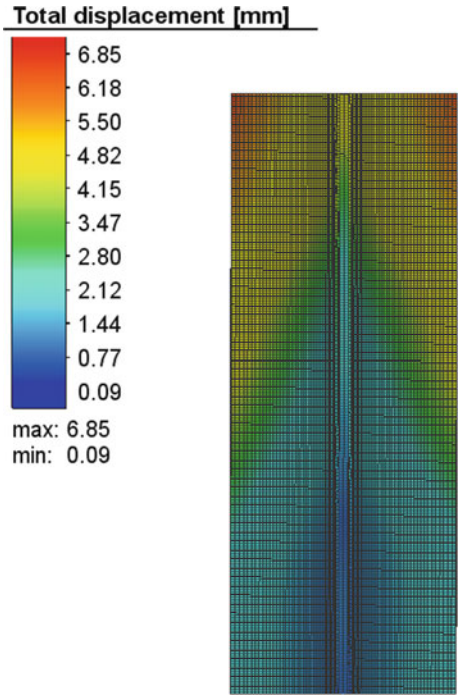

Fig. 19 Diagram of deformation after cooling for 15 min

5 Conclusion

According to the analysis of the experimental results of the numerical simulation of the welding process of three schemes, it is found that the selection of welding sequence has a very obvious effect on the deformation. In the actual welding process, for the T-joint fillet welding process, the most appropriate welding process should be cross-welding or symmetrical welding, and the deformation of the plate after welding is small. However, the welding process of scheme 2 will have a large deformation effect.

For the actual production process, in consideration of cost saving and human and material resources, the welding process of cross-back-welding is more used. In addition, the deformation gap between the two ends of the bottom plate in scheme II is large. Considering the factors, compression clamps can be applied on the left and right sides of the bottom plate, or fixed clamps with large pressure can be applied on the left side, i.e., the welding side first, so that the deformation gap between the left and right ends is small.

References

1. Wang JC, Yi B, Zhou H (2019) Prediction and control of welding induced buckling in reinforced thin plate ship structure. Naval Archi Ocean Eng 35(01):58–63
2. Zhao DS, Miao TJ, Wu LL, Liu YJ (2019) Experimental parameter design and calculation of welding deformation correction by flame straightening. Lab Sci 22(03):20–23
3. Zhang WY (1989) Theory of welding heat conductance. China Machine Press, Beijing, pp 1–6
4. Zhang X, Qu HY (2015) Simulation of local model multi-pass welding simulation based on SYSWELD. J Hebei United Univ 37(04):27–33 (Natural Science)
5. Zhao KL (2009) Study on simulation of welding deformation of hull blocks based on FEA. Harbin Engineering University
6. Ying CC (2013) Shipping technology. Shanghai: Shanghai Jiao Tong University press, pp 403–404
7. Mo LC, Qian BN, Guo XM, Yu SF (2001) The development of models about welding heat sources calculation. Weld J (03):93–96+101
8. John G (1984) A new finite model for welding heat source. Metall Trans 15B(2):299–305